Tissue Eng Regen Med (2022) 19(6):1321–1336
https://doi.org/10.1007/s13770-022-00471-3

Online ISSN 2212-5469

ORIGINAL ARTICLE

The Combination of Platelet Rich Plasma Gel, Human Umbilical Mesenchymal Stem Cells and Nanohydroxyapatite/polyamide 66 Promotes Angiogenesis and Bone Regeneration in Large Bone Defect

Wei Liu[1] · Yong Huang[2] · Daqian Liu[3] · Teng Zeng[1] · Jingzhe Wang[1] · Ang Li[3] · Dawei Wang[1] · Xiaoyu Wang[1]

Received: 25 January 2022 / Revised: 21 May 2022 / Accepted: 15 June 2022 / Published online: 8 September 2022

Abstract

BACKGROUND: In the present study, a novel tissue engineering bone graft including platelet rich plasma gel (PRP gel), human umbilical mesenchymal stem cells (HUMSCs) and nanohydroxyapatite/polyamide 66 (nHA-PA66) was constructed. We explored whether the composite scaffolds could enhance the angiogenesis and bone repair capacity in rat femoral large bone defect (LBD). This study aimed to provide evidence for the clinical application of the composite scaffold in LBD treatment.

METHODS: PRP was prepared, the platelets and growth factors were measured. HUMSCs were isolated and identified. the osteogenic capacity of PRP *in vitro* was measured. Then HUMSCs-PRP-gel/nHA-PA66 composite scaffolds were synthesized and observed. The proliferation and osteogenesis differentiation of HUMSCs on the composite scaffold was measured. The angiogenic capacity of PRP *in vitro* was measured by capillary-like tube formation assay. Finally, the angiogenesis and bone repair capacity of the composite scaffolds was measured in rat LBD.

RESULTS: PRP contained high level of platelets and growth factors after activation, and promoted osteogenic and angiogenic differentiation *in vitro*. The HUMSCs-PRP-gel/nHA-PA66 composite scaffold was porosity and promoted the proliferation and osteogenesis differentiation of HUMSCs. At 12th weeks, more micro-vessels and new bone were formed around the composite scaffolds compared with other groups, the defect was almost repaired.

CONCLUSION: Our study for the first time identified that the combination of PRP gel, HUMSCs and nHA-PA66 scaffold could significantly promote angiogenesis and bone regeneration in rat LBD, which may have implications for its further application in clinical LBD treatment.

Keywords Large bone defect · Angiogenesis · Osteogenesis · Platelet rich plasma · Nanohydroxyapatite/polyamide 66

1 Introduction

The reconstruction of large bone defect (LBD) caused by trauma, surgical excision of tumors and congenital malformation is still a challenging problem in orthopedic surgery [1]. In clinical, LBDs are always repaired by bone grafts, including autografts, allografts, vascularized bone grafts. However, the bone grafts have many drawbacks. Briefly, autografts are severely limited by bone availability, donor site morbidity and movement impairments [2]; allografts are less osteoinductive than autografts and risky in disease transmission and immunogenic response [3];

Wei Liu and Yong Huang are co-first authors.

✉ Xiaoyu Wang
xiaoyuwang@hrbmu.edu.cn

[1] Department of Orthopedic Surgery, The First Affiliated Hospital of Harbin Medical University, 23 Youzheng Street, Nangang District, Harbin 150001, Heilongjiang, China

[2] Department of Orthopedic Surgery, The Affiliated Hospital of Qinghai University, Xining, Qinghai, China

[3] Department of Orthopedic Surgery, The Second Affiliated Hospital of Harbin Medical University, Harbin, Heilongjiang, China

vascularized bone grafts need anastomotic technique and good vascular condition in the donor site.

Nowadays, the bone tissue engineering strategy has appeared as one of the most promising approaches for the treatment of bone defect [4, 5]. Three basic biologic elements are required for bone tissue engineering, including stem cells, extracellular scaffolds and biological factors for growth, osteogenesis and angiogenesis [6]. Mesenchymal stem cells (MSCs) are considered as important contributors in bone tissue engineering due to their potential for multilineage differentiation into various cell lineages, such as osteoblasts, chondrocytes and adipocytes. In recent years, several *in vitro* and *in vivo* studies have proposed the application of MSCs in bone defect repair [7]. Bone marrow (BM)-derived MSCs were discovered first, and the bone marrow was considered the main source of MSCs for clinical application. However, bone marrow aspiration always causes pain at the puncture point and the source of BM-derived MSCs is limited. Previous study has demonstrated human umbilical mesenchymal stem cells (HUMSCs) can be utilized as alternative stem cells in the reconstruction and regeneration of bone defects [8]. In the present study, HUMSCs were considered as substitute cells for BM-derived MSCs and served as appropriate stem cells in bone tissue engineering.

With regard to the scaffold used in bone tissue engineering, inorganic hydroxyapatite (HA) and organic polymers constituted by various composite materials have been explored as bone graft substitutes over the years [9]. The nanohydroxyapatite/polyamide 66 (nHA-PA66) scaffold is a composite material of nanohydroxyapatite and polyamide 66, which is similar to an apatite blend with collagen organisms as natural bone. The scaffold is a good candidate as a bone graft substitute. Many studies have reported satisfactory clinical outcomes of the scaffold [10]. In our previous study [11], nHA-PA66 scaffold combined with LvNell-1 gene modified MSCs was implanted in the rat femoral LBD with severe periosteal damage. The results showed that new bone tissues had successfully grown into the defect areas. However, the study is far from ideal because the nHA-PA66 scaffold itself lacks osteoinductivity and the genetically modified biologics have the problem of bio-safety.

Compromised bone repair and regeneration in many patients can be attributed to impaired blood supply [12]. Platelet-rich plasma (PRP), which can be obtained by centrifuging the whole blood, has a platelet concentration 3–10 times higher than the whole blood (higher than 1×10^9 platelets/ml). After activation, PRP will release a pool of growth factors which have the functions of bone formation and vascularization, including platelet-derived growth factor (PDGF), transforming growth factor beta (TGF-β), vascular endothelial growth factor (VEGF, essentially VEGFA) [13]. In 1998, it was used in the initial stage of enhanced fracture healing [14]. Nowadays, PRP has been widely used in orthopedics to promote bone regeneration [15].

There are no studies that evaluate the performance of PRP in combination with HUMSCs and nHA-PA66 scaffold to repair LBD. In our study, we utilized precise motor-driven drilling machine to make LBD in rat femur. We explored whether the combination of PRP gel, HUMSCs and nHA-PA66 scaffold could enhance the angiogenesis and bone repair capacity in LBD. This study aimed to provide evidence for the clinical application of HUMSCs-PRP-gel/nHA-PA66 composite scaffold in the LBD treatment.

2 Materials and methods

2.1 Experimental animals

Male sprague dawley (SD) rats in our study were ordered from the experimental animal center of the Second Affiliated Hospital of Harbin Medical University (Harbin, Heilongjiang, China), housed in groups of four and gave five days to acclimate to the housing facility. Environmental conditions were a temperature of 22 ± 2 °C, humidity of 55% and natural light–dark cycle. Animals were housed in 600 × 380 × 200 mm^3 cages and gave access to rat maintenance food and water ad libitum. During housing, animals were monitored twice daily for health status. No adverse events were observed. All procedures were carried out under an approval of the Animal Care and Use Committee of Harbin Medical University (IACUC no. 2022061). All sections of this report adhere to the ARRIVE Guidelines 2.0 for reporting animal research [16]. A completed ARRIVE guidelines checklist is included in supplement S1.

2.2 PRP preparation

60 male SD rats weighed (mean ± SD) 312 ± 23 g were anesthetized with 10% chloral hydrate and then humanely euthanized. Study was conducted using 5 animals as one experimental unit. The whole blood was collected via heart puncture. The blood was anticoagulated with 3% acid-citrate dextrose (1/10 volume) and centrifuged for 15 min at 800 rpm at 20 °C. Then the upper plasma was collected into a new tube and centrifuged again for 15 min at 2000 rpm at 20 °C. The upper layer was called platelet poor plasma (PPP) and removed, leaving the PRP and buffy coat. Then the PRP was resuspended in the bottom.

2.3 PRP extract preparation, measurement of platelets and growth factors

The concentrations of platelets in PRP and whole blood were counted with an automated hematology analyzer (Nikon, Tokyo, Japan). Then PRP was stored at − 80 °C overnight and melted at 4 °C to release the factors from the concentrated platelets. Each sample was centrifuged at 1300 rpm for 10 min and the clear, cell-free supernatant was collected and stored at − 80 °C as PRP extract. The PRP extract was prepared for *in vitro* experiment. The concentrations of vascular endothelial growth factor (VEGF), platelet-derived growth factor (PDGF) and transforming growth factor-β (TGF-β) in PRP extract and whole blood were measured with ELISA according to the manufacturer's instructions (Shanghai Enzyme-linked Biotechnology Co., Ltd. Shanghai, China).

2.4 Isolation, expansion, immunophenotyping and osteogenic differentiation of HUMSCs

Human umbilical mesenchymal stem cells (HUMSCs) were purchased from Zhong Qiao Xin Zhou Biotechnology Co., Ltd (Shanghai, China) and were maintained in the HUMSCs complete medium (Zhong Qiao Xin Zhou Biotechnology Co.,Ltd. Shanghai, China). Culture medium was changed every 2–3 days, and cells were passaged when they reached to 80% confluence. Experiments were performed using cells between passages 2 and 4.

For the immunophenotyping of cells, monolayer cultured cells were detached by mechanical scratching and filtered through a stainless-steel mesh filter to eliminate cell aggregates from the single-cell suspension. After centrifugation, cells were blocked with 1% bovine serum albumin for 15 min. Table 1 describes the antibodies and antibody mixes. Cells were then incubated with 5 μL of antibodies for 30 min on ice. Appropriate isotype control antibodies were used to exclude nonspecific binding. After washing, the samples were analysed using a BD FACSCalibur (BD Biosciences, San Jose, CA, USA).

To induce osteogenic differentiation, cells were treated with PRP extract and induced with osteogenic medium, 7 days for ALP assay and 14 days for alizarin red staining. ALP staining and ALP activity were assessed according to the manufacturer's instructions (ALP kit, Nanjing Jiancheng, China). For alizarin red staining, cells were stained with 40 mM of Alizarin Red S solution (pH 4.1–4.4). 10% cetylpyridinium chloride (in 10 mM sodium phosphate, pH 7.0) was used to destrain the cells and the absorbance was measured at 562 nm by a microplate spectrophotometer. All experiments were performed in quintuplicate.

Table 1 List of antibodies used for flow cytometry validation

Antibody	Fluorophore	Company	Catalog number
CD34	APC	Abcam	Ab155377
CD45	FITC	Abcam	Ab27287
CD73	APC	Abcam	Ab155378
CD105	FITC	Abcam	Ab18278

APC allophycocyanin, FITC fluorescein isothiocyanate

2.5 Western blot analysis

Cultured cells were harvested by RIPA buffer. The total protein samples were quantified by BCA protein assay and layered by SDS-PAGE (10% polyacrylamide gels) and transferred to NC membranes (Millipore, Burlington, MA, USA), and the membranes were then blocked by PBST buffer containing 5% bovine serum albumin for 1 h. Subsequently, The membranes were then incubated overnight with collagen I antibody (cat. AF7001, dilution, 1:500, Affinity Biosciences Inc., Cincinnati, OH, USA) and osteocalcin antibody (cat. DF12303, dilution, 1:500, Affinity Biosciences Inc.), followed by application of goat anti-rabbit HRP conjugate antibodies (cat. AP132P, dilution, 1:2000, Millipore). The membrane was developed by the use of a Tanon-5200 detection kit (Tanon Technologies Inc., Shanghai, China) with GAPDH (cat. A19056, ABclonal Technology Co., Ltd., Wuhan, China) as a control. The bands were visualized and quantitated using Tanon GIS image processing system. All experiments were performed in quintuplicate.

2.6 RNA isolation and real–time quantitative PCR (RT—qPCR)

The expression levels of osteocalcin (OCN), collagen 1A1(COL1A1) in stem cells, VEGF, PDGF and TGF-β in the tissues were examined by RT—qPCR. Briefly, total RNA was extracted with Trizol reagent (Invitrogen, Carlsbad, CA, USA), 1 μg of total RNA was reverse—transcribed into cDNA with Transcriptor First Strand cDNA Synthesis Kit (Roche diagnostics Gmbh, Roche Applied Science, Mannheim, Germany) according to the manufacturer's instructions. Quantitative real-time PCR analysis of genes was conducted using ABI Prism 7300 real—time PCR system (Applied Biosystems, Waltham, MA, USA). The reaction was performed at 95 °C for 30 s; 40 cycles at 95 °C for 5 s, 55 °C for 30 s; and 4 °C for $+\infty$. $2^{-\Delta\Delta Cq}$ method was used to quantify relative gene expression. The primer sequences used in experiments of osteogenic differentiation of HUMSCs *in vitro* were as follows: OCN, 5′-CCCAGGCGCTACCTGTATCA-3′ (forward) and 5′-

GTGGTCAGCCAACTCGTCAC-3′ (reverse); COL1A1, 5′-CCTGTCTGCTTCCTGTAAACTC-3′ (forward) and 5′-GTTCAGTTTGGGTTGCTTGTC -3′ (reverse); β-Actin 5′-TGGCACCCAGCACAATGAA-3′ (forward) and 5′-CTAAGTCATAGTCCGCCTAGAA-3′ (reverse). The primer sequences used *in vivo* were as follows: VEGFA, 5′-GGATCAAACCTCACCAAAGCCA-3′ (forward) and 5′-TGGTCTGCATTCACATCTGCT-3′ (reverse); PDGF-B, 5′-CTACCTGCGTCTGGTCAGC-3′ (forward) and 5′-GCTCAGCCCCATCTTCGTCTAC-3′ (reverse); TGF-β1, 5′-GGCTGAACCAAGGAGACGGA-3′ (forward) and 5′-CCTCGACGTTTGGGACTGAT-3′ (reverse); GAPDH, 5′-TCTCTGCTCCTCCCTGTTCTA-3′ (forward) and 5′-GGTAACCAGGCGTCCGATAC-3′ (reverse). All experiments were performed in quintuplicate.

2.7 Scaffold preparation and HUMSCs seeding

The nHA-PA66 scaffold was synthesized as previously described [17]. Briefly, nHA-PA66 powders were mixed with ethanol at room temperature, the ratio of composite to ethanol (w:v) was varied from 0.6 to 0.8. Then the mixture was cast into the Teflon® mould and moved into oven at 80°C for 3 days. During this period, phase inversion of ethanol was thermally induced and the inter connective porous structure of the scaffold was gradually formed. After ethanol gradually evaporated from the mould, the material became solidification. The porous scaffold was finally obtained after being dried at 100 °C. The scaffold was cut into small pieces ($5 \times 5 \times 5$ mm^3) for cell culture and animal experiment and sterilized using ethylene oxide gas. The PRP and cell suspension at a density of 1×10^7 cells/ml were mixed at a volume ratio of 4:1 to obtain cell—PRP mixture at a density of 2×10^6 cells/ml, as described by Tajima et al. [18]. 30 µL of cell—PRP mixture was dripped onto each scaffold. Controls were established without PRP. MSCs suspensions at a density of 2×10^6 cells/ml were seeded. The constructs were incubated at 37 °C for 2 h to allow for cell diffusion and attachment. Then, 6 µL of thrombin was added onto the composite scaffold. All scaffolds were cultured statically for up to 7 days in an osteogenic induction medium. The medium was changed every 3 days.

2.8 Porosity measurement

After the composite scaffolds were cultured for 24 h, the porosity of the scaffold was measured by liquid displacement as previously described [19]. Ethanol was chosen as the displacing liquid because it easily penetrated into the pores of the scaffold without destroying the scaffold. The scaffold was immersed in a known volume (V1) of ethanol until the scaffold was completely saturated. The total volume of ethanol and ethanol—saturated scaffold was recorded as V2. The saturated scaffold was then removed carefully and the volume of residual ethanol was recorded as V3. Therefore, the volume of the saturated scaffold was V2–V3 and the volume of ethanol within the scaffold was V1–V3.

The porosity of the scaffold was calculated as follows.

$$\text{Porosity}\ (\%) = (\text{V1} - \text{V3}) / (\text{V2} - \text{V3}) \times 100$$

The experiments were performed 5 times and the average porosity value was obtained.

2.9 Scanning electron microscopy (SEM) observation

After the composite scaffolds were cultured for 24 h, the samples were taken out and rinsed with phosphate buffered saline (PBS) three times. Then the samples were immobilized with 2.5% (v/v) glutaraldehyde solution at 4 °C for 4 h, dehydrated with a graded series of ethanol (30, 50, 70, 90, and 100%), freeze-dried for 48 h. The samples were finally coated with gold. The morphology of the scaffold and the attachment of the cells were observed by scanning electron microscopy (HITACHI, Tokyo, Japan). The average ratio of fibrin coverage was calculate using NIH Image J software.

2.10 Cell proliferation and viability

The proliferation of HUMSCs on the scaffold was measured by using the MTT [3-(4,5-dimethylthiazol-2yl)-2,5-diphenyl-2H-tetrazolium bromide] assay after 1,

3, and 7 days of culture. The absorbance of the solution in each well was measured at 490 nm by a microplate spectrophotometer.

2.11 Alkaline phosphatase (ALP) assay

ALP was measured after 1, 3, 7 days of cell seeding. To assess the ALP activity, cells were lysed with 1% Triton X—100 in DEPC—treated water and three freeze–thaw cycles. ALP activity assay was assessed according to the manufacturer's instructions (ALP kit, Nanjing Jiancheng, China).

2.12 Endothelial cells (ECs) culture

60 SD rats weighed (mean ± SD) 312 ± 23 g were anesthetized with 10% chloral hydrate and then humanely euthanized. Study was conducted using 5 animals as one experimental unit. ECs isolation from the thoracic aorta were performed as described by Chen et al. [20]. The cells were cultured in DMEM supplemented with 15% (v/v) FBS, L—glutamine (2 mM), 100 µg/mL sodium heparin,

4 ng/mL VEGF, and 100 U penicillin/streptomycin at 37 °C in 5% CO_2. Once they had formed a monolayer, the cells were subcultured in DMEM with 10% FBS, digested with 2% trypsin, and collected.

2.13 Matrigel tube formation assay

The *in vitro* capillary—like tube formation assay was conducted using Matrigel™ Matrix (BD Biosciences) according to the manufacturer's instructions. Each well in 96—well plates was coated with 50 μL Matrigel, and the plates were incubated at 37 °C for 6 h to allow the Matrigel to polymerize fully. Cells after 24 h PRP extract co-culture were seeded at a density of 1.5×10^3 cells per well in the prepared plates and treated with 1.0 μM roxarsone for 6 h. Tube formation of each group was photographed from five random microscopic fields using an inverted light microscope (Leica, Wetzlar, Germany) and the average numbers and diameters of tubes per field were determined.

2.14 Rat femur large bone defect (LBD) model

The rats were anesthetized with 10% chloral hydrate. Large bone defect (LBD) of right femur was made as described by Henrich et al. [21]. The individual rat was considered the experimental unit within the studies. Briefly, the rats were placed in the left lateral prone position, and a 40 mm longitudinal incision was made over the lateral aspect of the right thigh. Then, the biceps femoris and vastus lateralis muscles were separated to expose the lateral aspect of the femoral bone. The LBD measuring 5 mm was created using a precise motor-driven drilling machine. The scaffold about $5 \times 5 \times 5$ mm^3, inserted by a 1.25 mm diameter K-wire, was implanted in the defect. The wound was irrigated with sterile saline, the muscles as well as the fascia were carefully repaired with 4–0 Vicryl sutures and the skin was closed with 3–0 silk suture. The operation was performed in the right femurs of rats weighed (mean ± SD) 148 ± 11 g. The rats with postoperative complications were excluded from the experiment, including incision infection (n = 2), incision rupture (n = 1), scaffold dislocation (n = 4) and K-wire dislocation (n = 2). A total of 50 animals were included in this study. Depending on the scaffold implanted in the defect area, the rats were randomly assigned to five experimental groups (n = 10 blank control, n = 10 nHA-PA66, n = 10 PRP-gel/nHA-PA66, n = 10 HUMSCs/nHA-PA66, n = 10 HUMSCs-PRP-gel/nHA-PA66). Random numbers were generated using the standard = RAND () function in Microsoft Excel. Rats were sacrificed at 6 and 12 weeks after implantation. The group allocation was blinded to the experimenters during the conduct of the experiment, the outcome assessment and the data analysis.

2.15 Micro-CT measurement

The samples were scanned using a micro-CT scanner (Skyscan 1076, Belgium) at 30 μm resolution. A constant volume of interest centered over the fracture site, with 150 slices thick (approximately 5 mm), was selected for analysis. The two dimensional images were reconstructed. The bone volume (BV, mm^3), bone volume density (BV/TV, %), and bone mineral density (g/cm^3) were calculated.

2.16 Histologic assessment

After decalcified in 10% EDTA for 2 weeks, all samples were fixed in 4% (v/v) neutral paraformaldehyde for 24 h after collection. Following dehydrated and embedded in paraffin, the tissues were cut into 5 μm sagittal sections. Then, the slides were stained with hematoxylin and eosin. The figures were examined and captured by another group of experienced histology researchers in a blinded manner using a microscope (Olympus, Tokyo, Japan). The histomorphometric analysis was conducted using NIH Image J software.

2.17 Statistical analysis

Statistical analysis was performed by using GraphPad Prism 9 software and SPSS. All data were expressed as mean ± SD. The data between two groups were compared using independent-samples t-test. The data between three or more groups were compared by the one-way ANOVA and Tukey test. $p < 0.05$ was considered to be statistically significant. The sample size in the studies was estimated as previously reported [5].

3 Results

3.1 Concentration of platelets and growth factors

Since each purification method may affect the chemical ingredients of PRP, we measured the concentrations of platelets and growth factors in the PRP prepared by our protocol. Results showed that the mean platelet count for PRP was $1.114 \pm 0.09 \times 10^6/\mu L$, while that of whole blood was $0.323 \pm 0.04 \times 10^6/\mu L$ (3.45 times higher in PRP as compared to whole blood). Correspondingly, PRP released 2.31 times higher VEGF, 2.27 times higher TGF-β and 3.19 times higher PDGF as compared to whole blood. All of these confirmed the presence of a increased

concentration of platelets and growth factors during the PRP preparation (Table 2).

3.2 Immunophenotyping identification of HUMSCs

To verify whether HUMSCs have been successfully cultured *in vitro*, we performed flow cytometry to detect the immunophenotyping of the cells. Results showed that CD 73 and CD 105 were positive among cells. However, CD 34 and CD 45 were barely positive among cells (Fig. 1). Thereby demonstrating a characteristic immunophenotype of HUMSCs.

3.3 PRP promotes osteogenic and angiogenic differentiation *in vitro*

The osteogenic capacity of PRP extract was measured by ALP staining, ALP activity assay, alizarin red staining, western blot analysis and RT—qPCR. After 7 days of osteogenic induction in osteogenic medium (OM), ALP positive cells were more prominent in OM + PRP group compared with OM group (Fig. 2). Correspondingly, the ALP activity of the OM + PRP group was significant higher than the OM group (Fig. 2A, $p < 0.001$). After 14 days of osteogenic induction, calcium mineral deposition was more prominent in OM + PRP group compared with OM group (Fig. 2). The quantitative analysis showed the absorbance of the OM + PRP group was significant higher than the OM group (Fig. 2B. $p < 0.5$). The relative mRNA and protein expression of COL 1 and OCN in OM + PRP group was significant higher than the OM group (Fig. 2E-G).

To further explore the angiogenic capacity of PRP *in vitro*, ECs with PRP extract were induced with angiogenic medium (AM) for 24 h. Figure 2 shows photographs of the capillary-like tubes that formed in the Matrigel tube formation assay. Compared to the AM group, PRP significantly increased the number of formed tubes in AM + PRP group (Fig. 2C, $p < 0.001$). Correspondingly, the average diameters of formed tubules were significantly decreased in AM + PRP group (Fig. 2D, $p < 0.01$). All of the results indicate that the PRP prepared by our protocol played an important role in the promotion of osteogenesis and angiogenesis *in vitro*.

Table 2 The concentrations of platelets and growth factors in PRP and whole blood (n = 5, mean ± SD)

Platelet and growth factors	PRP	Whole blood
Platelets (10^6/μL)	1.114 ± 0.09	0.323 ± 0.04
VEGF (pg/ml)	344.33 ± 27.8	149.19 ± 16.37
TGF-β (pg/ml)	119.72 ± 13.69	52.81 ± 10.99
PDGF (pg/ml)	2272.94 ± 125.49	712.60 ± 50.14

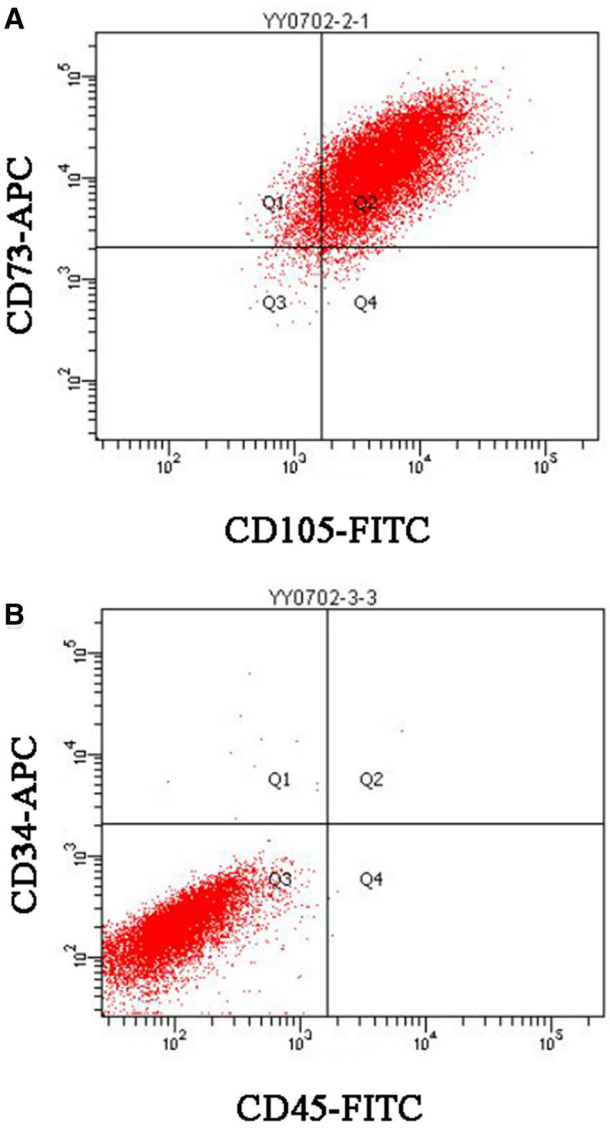

Fig. 1 Representative flow cytometry scatter plots, HUMSCs are a homogeneous population of cells and exhibit surface expression of standard cell surface markers. **A** Positive for CD 73 and CD 105. **B** Negative for CD 34 and CD 45

3.4 The structure of PRP with nHA-PA66 scaffold and cell attachment.

SEM analysis showed that the nHA-PA66 scaffolds were polyporous with an average pore diameter of 300—500 μm. Many small pores with diameters ranging from 50 μm to 100 μm could be seen in the wall of large pores. The scaffold had a rough surface (Fig. 3A). In PRP-gel/nHA-PA66 group, the PRP-gel filled the macropores and formed a smooth fibrin network (Fig. 3B). In HUMSCs/

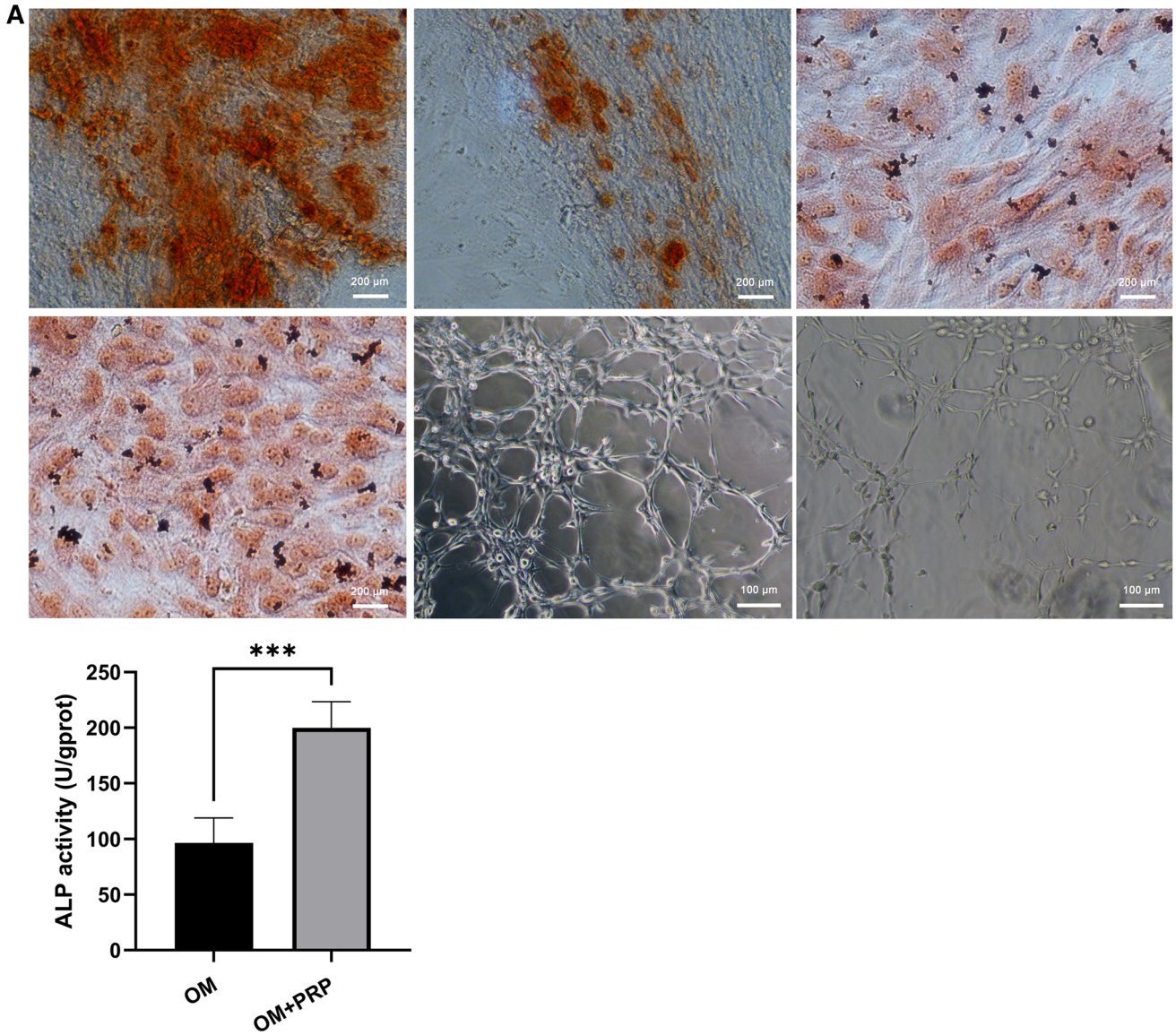

Fig. 2 PRP promotes osteogenic and angiogenic differentiation *in vitro*. The ALP-positive cells and calcium deposition was more prominent in OM + PRP group compared with OM group (40 ×). PRP significantly promoted the formation of capillary-like tubes in AM + PRP group. **A** ALP activity after 7 days of osteogenic induction. **B** Absorbance of alizarin red staining after 14 days of osteogenic induction. **C**, **D** The number and average diameters of formed tubes after 24 h of angiogenic induction. **E** Relative expression of COL1A1 and OCN mRNA after 14 days of osteogenic induction. **F**,**G** The protein expression of COL I and OCN after 14 days of osteogenic induction. (Data in mean ± SD, $n = 5$, $^{*}p < 0.5$, $^{**}p < 0.01$, $^{***}p < 0.001$, OM = osteogenic medium, AM = angiogenic medium)

nHA-PA66 group, the cells adhered to the surface of scaffold and had long protuberances (Fig. 3C). In HUMSCs-PRP-gel/nHA-PA66 group, the cells adhered to the surface of PRP gel and were more elongated and spread than that on the nHA-PA66 scaffold (Fig. 3D). The average porosity of the HUMSCs-PRP-gel/nHA-PA66 was 52.8%, and showed no statistically significant difference between the HUMSCs-PRP-gel/nHA-PA66 group and other groups (Fig. 3E). The average ratio of fibrin coverage was 66.5% in PRP-gel/nHA-PA66 group and 60.3% in HUMSCs-PRP-gel/nHA-PA66 group.

3.5 Cell proliferation *in vitro*

The absorbance values of the two groups increased with the extending of culture time. At day 1 after cell seeding, there was no significant difference between the two groups. At day 3 and 7 after cell seeding, the absorbance values of HUMSCs-PRP-gel/nHA-PA66 were significantly higher compared with that of the HUMSCs/nHA-PA66, indicating the PRP in the scaffold has a positive effect on the proliferation of HUMSCs (Fig. 4).

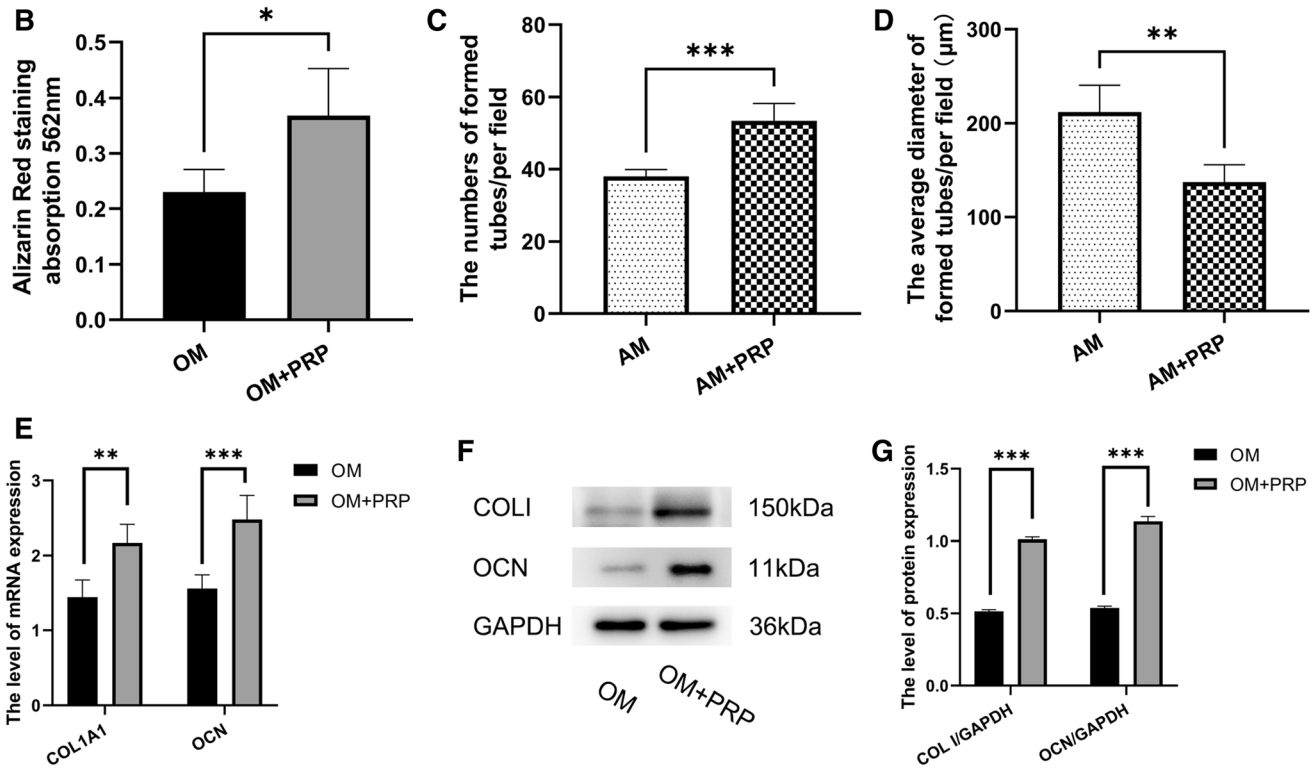

Fig. 2 continued

3.6 Cell osteogenic differentiation after co-culture

The ALP activity of the two groups increased with the extending of culture time. At 1 day after cell seeding, there was no significant difference between the two groups. At 3 and 7 days after seeding, significantly higher ALP activity was detected in the HUMSCs-PRP-gel/nHA-PA66 group when compared to the HUMSCs/nHA-PA66 group (Fig. 5).

3.7 HUMSCs-PRP-gel/nHA-PA66 scaffold significantly improves angiogenesis and bone regeneration in the LBD site

After femur LBD was successfully established in rat model, the HUMSCs-PRP-gel/nHA-PA66 scaffold was implanted in the defect (Fig. 6). The results of HE staining displayed that at 6 weeks after surgery, little new bone tissues were formed in defect only group, and most of the defect areas were filled with fibrous tissues in nHA-PA66 group and PRP-gel/nHA-PA66 group. But some micro-vessels had grown into the pores of scaffold in PRP-gel/nHA-PA66 group. The group of HUMSCs/nHA-PA66 formed some pieces of new bone around the scaffold. In HUMSCs-PRP-gel/nHA-PA66 group, micro-vessels and new bone formed around the scaffold and the bone defect was almost morphologically repaired (Fig. 7).

Compared with other groups, histomorphometric analysis showed the relative area of new bone tissue in repair area was increased significantly in both HUMSCs/nHA-PA66 and HUMSCs-PRP-gel/nHA-PA66 group. However, the increase of HUMSCs-PRP-gel/nHA-PA66 group was significantly higher than that of HUMSCs/nHA-PA66 group (Fig. 7A). The mean vessel density of both PRP-gel/nHA-PA66 group and HUMSCs-PRP-gel/nHA-PA66 group was increased significantly compared with other groups, but the increase between the two groups had no significant difference (Fig. 7B). At 6 weeks after surgery, the RT—qPCR results revealed that the expression level of PDGF-B, TGF-β1 and VEGFA mRNA was significantly increased in HUMSCs-PRP-gel/nHA-PA66 group compared with other groups. The increase between the PRP-gel/nHA-PA66 group and HUMSCs-PRP-gel/nHA-PA66 group had no significant difference.

Then we performed micro-CT to detect the bone formation among groups (Fig. 8). The results showed that even after 12 weeks, the bone defects were still existed and the gaps were not filled with bone tissues in the nHA-PA66 group and PRP-gel/nHA-PA66 group. Despite some new bone tissues were observed around the scaffolds in HUMSCs/nHA-PA66 group, the bone defect was still exist. In the HUMSCs-PRP-gel/nHA-PA66 group, the cortical bones were partial remodeled and the defect area was almost repaired. Quantitative parameters for new bone

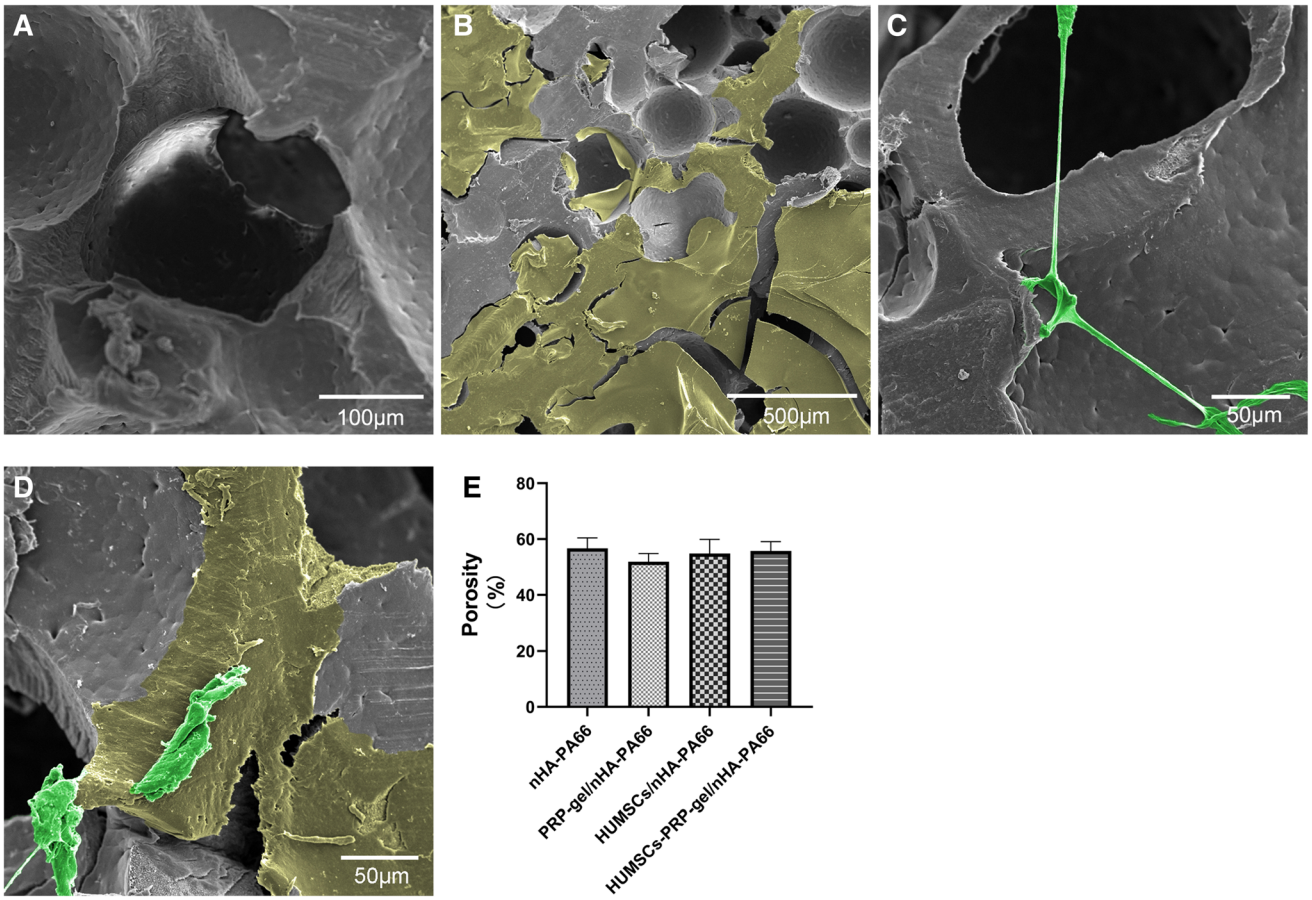

Fig. 3 The morphology of **A** nHA-PA66 scaffolds, **B** PRP-gel/nHA PA66, **C** HUMSCs/nHA-PA66 and **D** HUMSCs-PRP-gel/nHAPA66. The yellow areas represent the fibrin network formed by PRP gel. The green areas represent the stem cells adhered to the scaffolds. **E** The porosity of the scaffolds from the four groups. (Data in mean ± SD, $n = 5$)

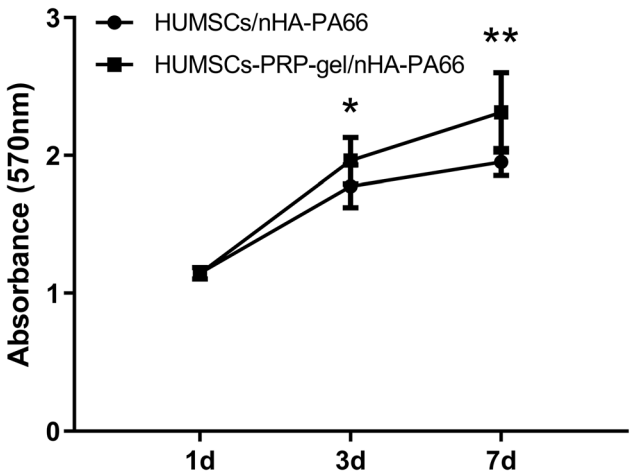

Fig. 4 MTT assay for cell proliferation *in vitro*. The HUMSCs-PRP-gel/nHA-PA66 group demonstrated significantly higher absorbance values compared with the HUMSCs/nHA-PA66 group at day 3 and 7. (Data in mean ± SD, $n = 5$, $^{*}p < 0.05$, $^{**}p < 0.01$)

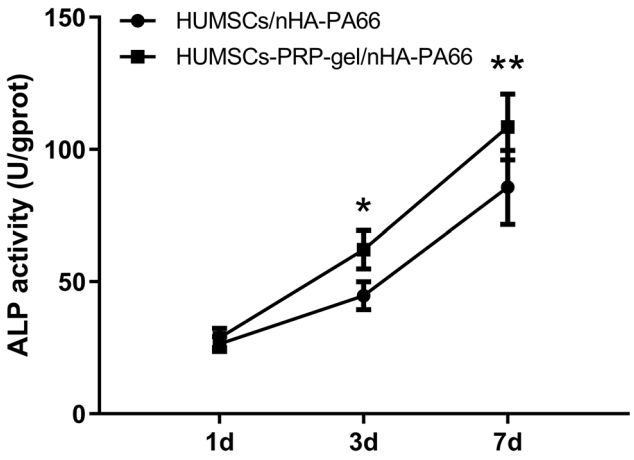

Fig. 5 ALP activity assay for cell osteogenic differentiation *in vitro*. The HUMSCs-PRP-gel/nHA-PA66 group demonstrated significantly higher ALP activity compared with the HUMSCs/nHA-PA66 group at day 3 and 7. (Data in mean ± SD, $n = 5$, $^{*}p < 0.05$, $^{**}p < 0.01$)

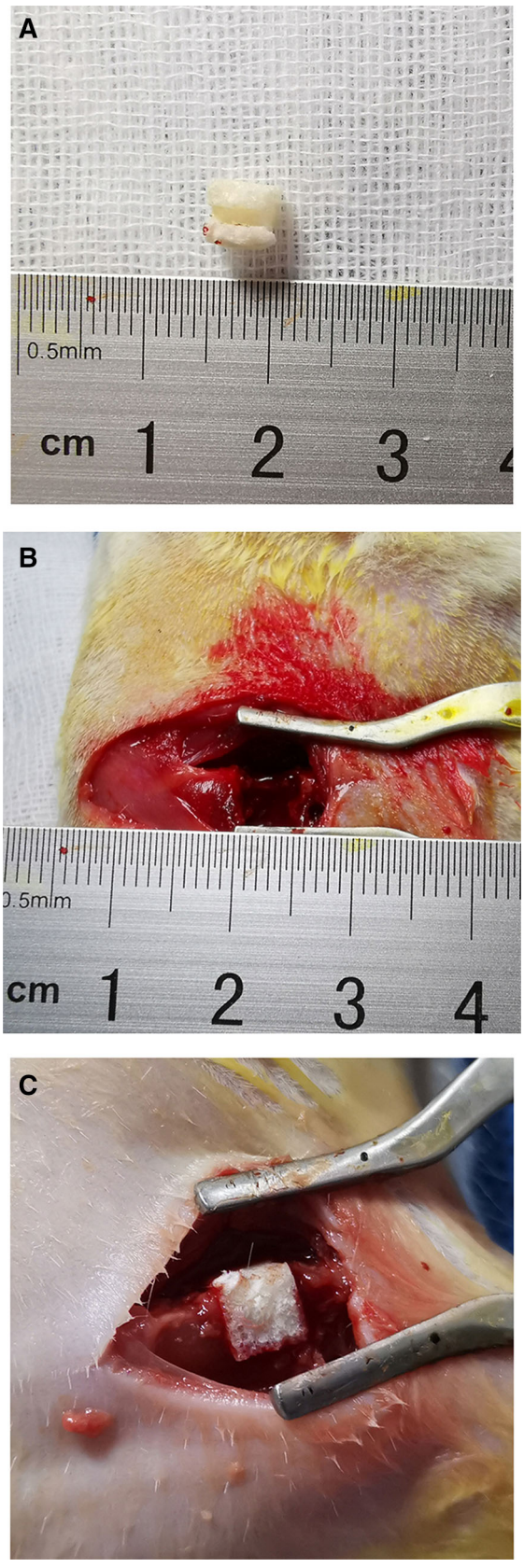

◀**Fig. 6** Surgical procedure for the implantation of scaffolds in rat femoral LBD site. **A** The scaffold was cut into 5 × 5 × 5 mm^3 before implantion. **B** Cylindrical LBD of 5 mm diameter and 5 mm depth was established in rat femur. **C** The scaffold could be accurately and stably filled into the femoral defect area

formation were obtained and statistically analyzed from the region of interest (ROI), including bone volume (BV, mm^3), bone volume density (BV/TV, %), and bone mineral density (g/cm^3). The results were illustrated in Fig. 8B–D. The HUMSCs-PRP-gel/nHA-PA66 group had more bone formation in defect area compared with other groups. All of the results indicated both HUMSCs and PRP were critical for angiogenesis and bone regeneration of LBD.

4 Discussion

The treatment of LBD remains a troublesome problem for orthopedic surgeons. Studies have reported that the critical size of LBD should be 1.5–2.5 times the diameter of bone or one-tenth of the bone length [22]. The average length of femoral bones of SD rats is about 4 cm. Therefore, to construct rat femoral LBD model, the length of defect should be more than 4 mm. In our experiment, cylindrical LBD of 5 mm depth was established in rat femur using a precise drilling device. In blank control group, at 12 weeks after bone defect operation, we found the bone defect was still exist and full of fibrous tissue. The result indicated that LBD in femoral bone of rat was successfully modeled. Even after 12 weeks, the defects could not be naturally healed, and the natural repair effect was poor. Thus, LBD is difficult to be healed by the intrinsic regenerative capacity of the bone and requires treatments to promote bone regeneration.

Compromised bone repair and regeneration in many patients can be attributed to impaired blood supply [23]. In present study, we developed a composite scaffold for the repairing of LBD in rat femur by combining activated PRP gel and HUMSCs onto the nHA-PA66 scaffolds. Our results demonstrated the efficiency of this composite scaffold in angiogenesis and bone regeneration, and emphasized the importance of PRP and HUMSCs for LBD treatment.

Compared to bone marrow—derived MSCs (BM—MSCs), HUMSCs have several advantages. Firstly, the umbilical cord blood (UCB) is often discarded after childbirth, so the collection of cord blood is easy and noninvasive; Secondly, the cord—blood units can be stored in advance and are therefore rapidly available when needed [24]; Finally, HUMSCs are considered less immunogenic compared to BM—MSCs, and thus less stringent human

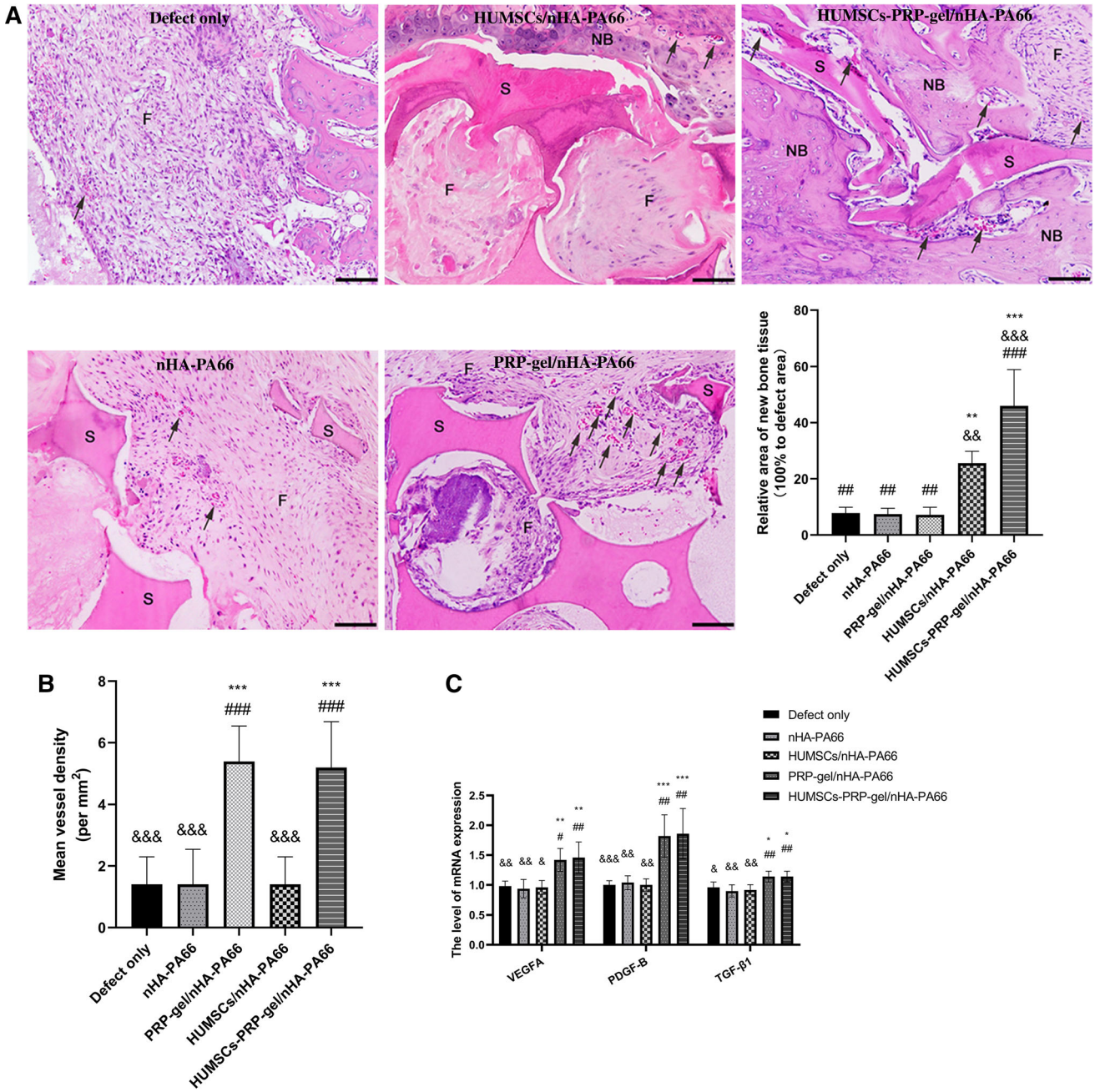

Fig. 7 HUMSCs-PRP-gel/nHA-PA66 significantly improved angiogenesis and morphological repair in bone defects at 6th week after surgery. **A** Relative area of new bone tissue in repair area. **B** Quantitative analysis of mean vessel density per mm^2. **C** Relative expression of PDGF-B, VEGFA and TGF-β1 mRNA in repair area. (3 randomized fields of view for each group. S: nHA-PA66 scaffold, NB: newly formed bone, F: fibrous and connective tissue, black arrows: microvessels, *Scale bar = 100* μm. Data in mean ± SD, $n = 5$, $^{*}p < 0.05$, $^{**}p < 0.01$, $^{***}p < 0.001$ versus Defect only group; $^{\&}p < 0.05$, $^{\&\&}p < 0.01$, $^{\&\&\&}p < 0.001$ versus PRP-gel/nHA-PA66 group; $^{\#}p < 0.05$, $^{\#\#}p < 0.01$, $^{\#\#\#}p < 0.001$ versus HUMSCs/nHA-PA66 group)

leukocyte antigen (HLA) matching is required [25]. HUMSCs have been demonstrated to possess osteogenic differentiation potential similar to that of BM—MSCs, and might be a preferable allogeneic source of MSCs for the treatment of difficult bone repair [26]. Liu et al. reported that pre-differentiated HUMSCs seeded on demineralized bone matrix (DBM) could lead to formation of mineralized bone like tissue in a rat calvarial defect model [27]. In the present study, the HUMSCs were purchased from biotechnology company and served as the stem cells in the composite scaffolds. The cell type was determined via immunophenotyping. Results displayed that these cells did not express hematopoietic lineage markers including CD 34 and CD 45, and were positive for CD 73, CD 105. In

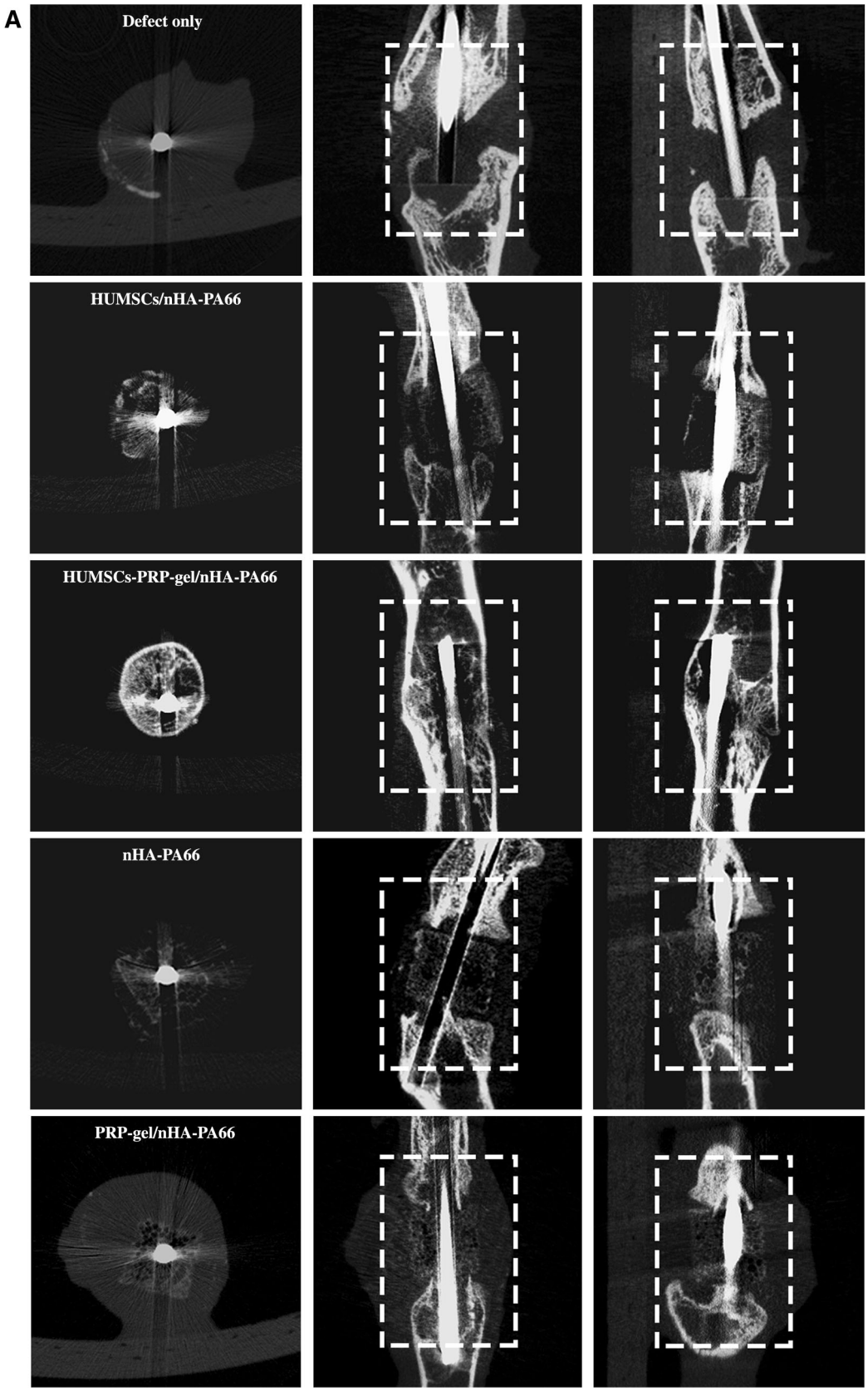
A
Defect only
HUMSCs/nHA-PA66
HUMSCs-PRP-gel/nHA-PA66
nHA-PA66
PRP-gel/nHA-PA66

◀**Fig. 8** **A** Two dimensional images by micro-CT of different groups at 12th week after surgery (dashed rectangles indicate bone defect sites). **B** Bone volume at 12th week after surgery. **C** Bone volume density at 12th week after surgery. **D** Bone mineral density of new bone tissues at 12th week after surgery. (3 randomized fields of view for each group, Data in mean ± SD, $n = 5$, $^{*}p < 0.05$, $^{***}p < 0.001$ versus Defect only group; $^{\&}p < 0.05$, $^{\&\&\&}p < 0.001$ *vs.* PRP-gel/nHA-PA66 group; $^{\#}p < 0.05$, $^{\#\#}p < 0.01$ versus HUMSCs/nHA-PA66 group)

addition, osteogenic differentiation of the cells was demonstrated. All results indicated that the seed cells in our study were not blood cells but HUMSCs [28].

PRP is abundant in fibrin and platelet containing a variety of growth factors which are released after activation. Previous study demonstrated PRP treatment induced the proliferation of MSCs and promoted the osteogenic differentiation of MSCs [29]. PRP combined with HUMSCs can also enhance bone regeneration *in vivo* [8]. Moreover, PRP are crucial for angiogenesis. Xu et al. reported that the PRP treatment was capable of increasing angiogenesis and re-epithelialization which was important for the improvement of skin wound healing [30].

PRP is defined as a fraction of the autologous plasma with high platelet concentration above the base line. Proper concentration of platelet is the key factor in the effectiveness of PRP therapy [31]. However, platelet count in PRP may different according to the preparation protocol and there is no international standard protocol for the preparation of PRP. Weibrich et al. reported that the best effects occurred when PRP with a platelet concentration of approximately 1,000,000/μL [32]. Marx et al. advised that the platelet count of PRP therapy should achieve a 2—6 fold increase over the whole blood [33]. In the present study, the PRP was all derived from SD rats, the weight and gender of rats were controlled, and the method was adapted from Ishida et al. [34]. The final platelet concentration was $1.114 \pm 0.09 \times 10^6$/μL (3.45 times higher in PRP as compared to whole blood) which was also consistent with previous literature. Both the preparation protocol of PRP and the results of platelet concentration confirmed the PRP used in our study is reliable.

The therapeutic actions of PRP derive from the release of a multitude of growth factors involved in tissue repair and regeneration. Among the PRP related growth factors, the PDGF, TGF-β and VEGF are known to play a critical role in cell proliferation, osteogenic differentiation and angiogenesis. PDGF stimulates specific target cells (endothelium, fibroblasts, macrophages and mesenchymal cells) by binding to cell surface receptors, and regulates collagenase secretion and collagen synthesis [31]. *In vitro*, PDGF enhances proliferation of multiple types of bone cells, including both osteoblast and osteoclast lineages [35]. TGF-β plays an important role in fracture healing and regeneration. In high concentration, it could enhance DNA synthesis of bone cells. Additionally, it could inhibit osteoclast formation and bone resorption [36]. In the remodeling phase of bone repair, TGF-β and PDGF are released from bone matrix during the process of bone resorption [32], which is required for angiogenesis and coordination of bone formation. VEGF plays important roles in proliferation, migration and activation of endothelial cells as well as in promotion of permeability and fenestration of blood vessels [37]. VEGF also participates in several stages of bone repair and regeneration [38].

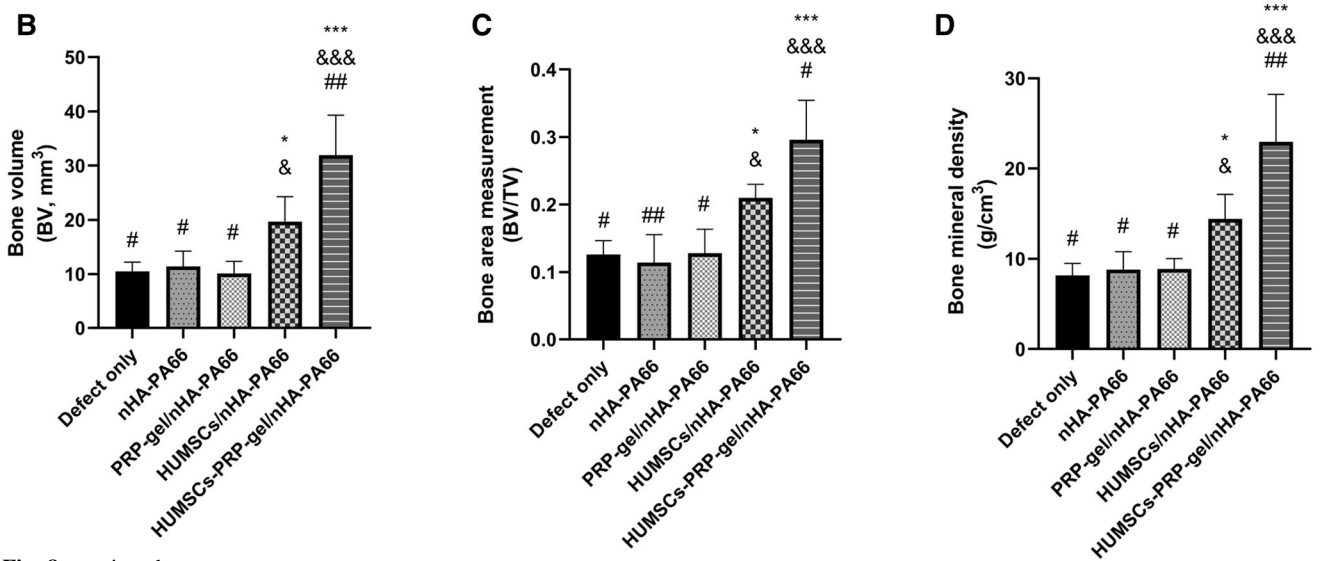

◀**Fig. 8** continued

In this study, we selectively detected the concentration of VEGF, PDGF and TGF-β in PRP extract using ELISA assay. Correspondingly with the concentration of platelet, VEGF was 2.49 times, PDGF was 2.97 times and TGF-β was 2.10 times increased over the concentration of the whole blood. Then we confirmed the osteogenic differentiation of HUMSCs by ALP activity, ALP staining and alizarin red staining. ALP is considered to be a marker in early state or pre-mature osteoblasts. After 7 days of osteogenic induction, ALP positive cells and ALP activity were more prominent in the environment with PRP extract. As a marker in later state of osteogenic differentiation, alizarin red staining showed the calcium mineral deposition was more prominent with PRP extract. The data provided a reasonable explanation for the positive results of the present study.

To further elucidate the osteogenic effect of PRP, we analyzed the expression of genes that characterizes the process of osteogenesis. Type I collagen (COL I) is one of the earliest osteoblast markers and the most abundant component of the immature bone matrix. The gene starts to be expressed in immature osteoprogenitors and lasts during the whole differentiation process, and TGF-β and PDGF are able to upregulate COL1A1 [39]. In this study, COL1A1 was highly expressed with PRP extract, indicating the promotion of early stage of osteogenesis. OCN is a mature osteoblast marker that influences hydroxyapatite formation [40], and increases in the late stage of osteogenesis [41]. Our results indicated OCN gene appears to be overexpressed after 14 days of treatment with PRP extract, suggesting the promotion of late stage of osteogenesis.

With regard to grafting scaffold combined with PRP, several studies have evaluated the effect of PRP in combination with nHA scaffold. Sadeghinia et al. reported that the nano-hydroxy apatite/chitosan/gelatin scaffolds treated with fibrin glue and activated PRP showed a fibrin network, and increased the osteogenic differentiation of human dental pulp stem cells [42]. In the present study, we demonstrated the nHA-PA66 scaffold was characterized with high porosity and had a three-dimensional microstructure similar to natural bone, indicating the scaffold had good bone conductibility. The PRP-gel adhered to the scaffold formed a fibrin network, preventing the cells from falling off the scaffold after seeding. Both proliferation and osteogenic differentiation of HUMSCs were significantly improved with the introduction of PRP. Our results indicated the PRP gel could provided a bioactive and adhensive surface for the attachment, proliferation and osteogenic differentiation of stem cells.

In the skeletal system, blood vessels regulate developmental and regenerative bone formation. Increasing study has found that the key factor contributing to difficult repair of LBD is poor vascularization [43]. *In vitro* study, our results indicated that PRP extract could significantly promote the formation of capillary-like tubes of endothelial cells. *In vivo* study, our results indicated the use of PRP in defects facilitate the release of VEGF, PDGF and TGF-β into local environment, which were highly beneficial for neovascular formation. The newly formed blood vessels grew around the scaffolds in PRP-gel/nHA-PA66 group and HUMSCs-PRP-gel/nHA-PA66 group. Without the combination of PRP gel, the neovascular formation in HUMSCs/nHA-PA66 group was significantly decreased. However, the effect on bone regeneration in PRP-gel/nHA-PA66 group was not significantly superior to that of HUMSCs-PRP-gel/nHA-PA66 group, which indicated the importance of HUMSCs in the composite scaffold. The vascularization facilitates delivery of oxygen, nutrients and growth factors to the construct and increases the volume of tissue-engineered bone. The PRP related signals also enhance the osteogenic potential of stem cells. The HUMSCs acted as seed cells and the PRP related VEGF, PDGF and TGF-β acted as signal factors. The combination of seed cells and signal factors significant promoted neovascular formation and bone regeneration. Owing to the positive effect of PRP related growth factors and HUMSCs on osteogenesis and angiogenesis, the combination of PRP-gel/nHA-PA66 scaffold with HUMSCs induced the strongest bone regenerative response and greatly accelerated bone regeneration compared with other groups. The limitation of the study is that there is no international standard protocol for the preparation of PRP. In a future study, we intend to study about the main component in PRP according to the different gender, age, genetic background and preparation protocol, and the cross-interactions of the PRP related growth factors.

Our findings support the use of PRP as an effective way in bone tissue engineering to improve vascularization and bone regeneration. A combination of HUMSCs with PRP-gel on nHA/PA66 scaffold provides the three essential factors of ideal bone graft substitutes: stem cells for osteogenesis, growth factors for osteoinduction and scaffold for osteoconduction. This is the first report, to our knowledge, of effective transplantation of HUMSCs-PRP-gel/nHA-PA66 scaffold to promote bone regeneration in the LBD repair. The results of our study may have clinical implications for its further application in the LBD treatment.

Supplementary Information The online version contains supplementary material available at https://doi.org/10.1007/s13770-022-00471-3.

Acknowledgements The authors wish to thank Professor Lei Yang from Harbin Medical University, China, for the technical help and helpful discussion. We also gratefully acknowledge the core facilities and software provided by the Orthopedic Diagnosis and Treatment

Center of the First Affiliated Hospital of Harbin Medical University, China.

Funding This work was funded by Heilongjiang Provincial Postdoctoral Science Foundation, China (No.LBH-Z18202).

Declarations

Conflicts of interest The authors declare that they have no competing interests.

Ethical statement The animal studies were performed after receiving approval of the Institutional Animal Care and Use Committee (IACUC) in Harbin Medical University (IACUC no. 2022061)

References

1. Vidal L, Kampleitner C, Brennan MÁ, Hoornaert A, Layrolle P. Reconstruction of large skeletal defects: current clinical therapeutic strategies and future directions using 3D printing. Front Bioeng Biotechnol. 2020;8:61.
2. Dimitriou R, Mataliotakis GI, Angoules AG, Kanakaris NK, Giannoudis PV. Complications following autologous bone graft harvesting from the iliac crest and using the RIA: a systematic review. Injury. 2011;42:S3-15.
3. Berner A, Reichert JC, Müller MB, Zellner J, Pfeifer C, Dienstknecht T, et al. Treatment of long bone defects and non-unions: from research to clinical practice. Cell Tissue Res. 2012;347:501–19.
4. Zhang LY, Bi Q, Zhao C, Chen JY, Cai MH, Chen XY. Recent advances in biomaterials for the treatment of bone defects. Organogenesis. 2020;16:113–25.
5. Cui Y, Zhu T, Li A, Liu B, Cui Z, Qiao Y, et al. Porous particle-reinforced bioactive gelatin scaffold for large segmental bone defect repairing. ACS Appl Mater Interfaces. 2018;10:6956–64.
6. Toosi S, Behravan N, Behravan J. Nonunion fractures, mesenchymal stem cells and bone tissue engineering. J Biomed Mater Res A. 2018;106:2552–62.
7. Kangari P, Talaei-Khozani T, Razeghian-Jahromi I, Razmkhah M. Mesenchymal stem cells: amazing remedies for bone and cartilage defects. Stem Cell Res Ther. 2020;11:492.
8. Wen Y, Gu W, Cui J, Yu M, Zhang Y, Tang C, et al. Platelet-rich plasma enhanced umbilical cord mesenchymal stem cells-based bone tissue regeneration. Arch Oral Biol. 2014;59:1146–54.
9. Zhang Y, Deng X, Jiang D, Luo X, Tang K, Zhao Z, et al. Long-term results of anterior cervical corpectomy and fusion with nano-hydroxyapatite/polyamide 66 strut for cervical spondylotic myelopathy. Sci Rep. 2016;6:26751.
10. Hu B, Wang L, Song Y, Hu Y, Lyu Q, Liu L, et al. A comparison of long-term outcomes of nanohydroxyapatite/polyamide-66 cage and titanium mesh cage in anterior cervical corpectomy and fusion: A clinical follow-up study of least 8 years. Clin Neurol Neurosurg. 2019;176:25–9.
11. Wang X, Ju F, Li A, Geng S, Sun J, Liu R, et al. Nell-1 gene modified mesenchymal stem cells on biomimetic porous nano-hydroxyapatite/polyamide 66 scaffolds effectively prevent non-union in rats. J Biomat Tissue Eng. 2016;6:408–16.
12. Fan H, Zeng X, Wang X, Zhu R, Pei G. Efficacy of prevascularization for segmental bone defect repair using β-tricalcium phosphate scaffold in rhesus monkey. Biomaterials. 2014;35:7407–15.
13. Meheux CJ, McCulloch PC, Lintner DM, Varner KE, Harris JD. Efficacy of intra-articular platelet-rich plasma injections in knee osteoarthritis: a systematic review. Arthroscopy. 2016;32:495–505.
14. Marx RE, Carlson ER, Eichstaedt RM, Schimmele SR, Strauss JE, Georgeff KR. Platelet-rich plasma: growth factor enhancement for bone grafts. Oral Surg Oral Med Oral Pathol Oral Radiol Endod. 1998;85:638–46.
15. Xie H, Cao L, Ye L, Du J, Shan G, Hu J, et al. Autogenous bone particles combined with platelet-rich plasma can stimulate bone regeneration in rabbits. Exp Ther Med. 2020;20:279.
16. Percie du Sert N, Hurst V, Ahluwalia A, Alam S, Avey MT, Baker M, et al. The ARRIVE guidelines 2.0: Updated guidelines for reporting animal research. PLoS Biol. 2020;18:e3000410.
17. Wang H, Li Y, Zuo Y, Li J, Ma S, Cheng L. Biocompatibility and osteogenesis of biomimetic nano-hydroxyapatite/polyamide composite scaffolds for bone tissue engineering. Biomaterials. 2007;28:3338–48.
18. Tajima N, Sotome S, Marukawa E, Omura K, Shinomiya K. A three-dimensional cell-loading system using autologous plasma loaded into a porous β-tricalcium-phosphate block promotes bone formation at extraskeletal sites in rats. Mater Sci Eng, C. 2007;27:625–32.
19. Qi XN, Mou ZL, Zhang J, Zhang ZQ. Preparation of chitosan/silk fibroin/hydroxyapatite porous scaffold and its characteristics in comparison to bi-component scaffolds. J Biomed Mater Res A. 2014;102:366–72.
20. Chen S, Xu J, Wei Q, Zhao Z, Chen X, Cui H, et al. VEGF/Flk1 mechanism is involved in roxarsone promotion of rat endothelial cell growth and B16F10 xenograft tumor angiogenesis. Sci Rep. 2019;9:17417.
21. Henrich D, Seebach C, Nau C, Basan S, Relja B, Wilhelm K, et al. Establishment and characterization of the Masquelet induced membrane technique in a rat femur critical-sized defect model. J Tissue Eng Regen Med. 2016;10:E382–96.
22. Schmitz JP, Hollinger JO. The critical size defect as an experimental model for craniomandibulofacial nonunions. Clin Orthop Relat Res. 1986;205:299–308.
23. Wang C, Lu WW, Wang M. Multifunctional fibrous scaffolds for bone regeneration with enhanced vascularization. J Mater Chem B. 2020;8:636–47.
24. Malgieri A, Kantzari E, Patrizi MP, Gambardella S. Bone marrow and umbilical cord blood human mesenchymal stem cells: state of the art. Int J Clin Exp Med. 2010;3:248–69.
25. Rocha V, Labopin M, Sanz G, Arcese W, Schwerdtfeger R, Bosi A, et al. Acute leukemia working party of European blood and marrow transplant group: Eurocord-Netcord registry. Transplants of umbilical-cord blood or bone marrow from unrelated donors in adults with acute leukemia. N Engl J Med. 2004;351:2276–85.
26. Bougioukli S, Saitta B, Sugiyama O, Tang AH, Elphingstone J, Evseenko D, et al. Lentiviral gene therapy for bone repair using human umbilical cord blood-derived mesenchymal stem cells. Hum Gene Ther. 2019;30:906–17.
27. Liu G, Li Y, Sun J, Zhou H, Zhang W, Cui L, et al. In vitro and in vivo evaluation of osteogenesis of human umbilical cord blood-derived mesenchymal stem cells on partially demineralized bone matrix. Tissue Eng Part A. 2010;16:971–82.
28. Cui L, Bao H, Liu Z, Man X, Liu H, Hou Y, et al. HUMSCs regulate the differentiation of ovarian stromal cells via TGF-β1/Smad3 signaling pathway to inhibit ovarian fibrosis to repair ovarian function in POI rats. Stem Cell Res Ther. 2020;11:386.
29. Qi Y, Niu L, Zhao T, Shi Z, Di T, Feng G, et al. Combining mesenchymal stem cell sheets with platelet-rich plasma gel/calcium phosphate particles: a novel strategy to promote bone regeneration. Stem Cell Res Ther. 2015;6:256.

30. Xu P, Wu Y, Zhou L, Yang Z, Zhang X, Hu X, et al. Platelet-rich plasma accelerates skin wound healing by promoting re-epithelialization. Burns Trauma. 2020;8:tkaa028.
31. Everts P, Onishi K, Jayaram P, Lana JF, Mautner K. Platelet-rich plasma: new performance understandings and therapeutic considerations in 2020. Int J Mol Sci. 2020;21:7794.
32. Weibrich G, Hansen T, Kleis W, Buch R, Hitzler WE. Effect of platelet concentration in platelet-rich plasma on peri-implant bone regeneration. Bone. 2004;34:665–71.
33. Marx RE. Platelet-rich plasma: evidence to support its use. J Oral Maxillofac Surg. 2004;62:489–96.
34. Ishida K, Kuroda R, Miwa M, Tabata Y, Hokugo A, Kawamoto T, et al. The regenerative effects of platelet-rich plasma on meniscal cells in vitro and its in vivo application with biodegradable gelatin hydrogel. Tissue Eng. 2007;13:1103–12.
35. Colciago A, Celotti F, Casati L, Giancola R, Castano SM, Antonini G, et al. In Vitro Effects of PDGF Isoforms (AA, BB, AB and CC) on migration and proliferation of SaOS-2 osteoblasts and on migration of human osteoblasts. Int J Biomed Sci. 2009;5:380–9.
36. Doucet C, Ernou I, Zhang Y, Llense JR, Begot L, Holy X, et al. Platelet lysates promote mesenchymal stem cell expansion: a safety substitute for animal serum in cell-based therapy applications. J Cell Physiol. 2005;205:228–36.
37. Hu K, Olsen BR. Osteoblast-derived VEGF regulates osteoblast differentiation and bone formation during bone repair. J Clin Invest. 2016;126:509–26.
38. Tang Y, Wu X, Lei W, Pang L, Wan C, Shi Z, et al. TGF-beta1 induced migration of bone mesenchymal stem cells couples bone resorption with formation. Nat Med. 2009;15:757–65.
39. Glueck M, Gardner O, Czekanska E, Alini M, Stoddart MJ, Salzmann GM, et al. Induction of osteogenic differentiation in human mesenchymal stem cells by crosstalk with osteoblasts. Biores Open Access. 2015;4:121–30.
40. Tsao YT, Huang YJ, Wu HH, Liu YA, Liu YS, Lee OK. Osteocalcin mediates biomineralization during osteogenic maturation in human mesenchymal stromal cells. Int J Mol Sci. 2017;18:159.
41. Wang L, Li ZY, Wang YP, Wu ZH, Yu B. Dynamic expression profiles of marker genes in osteogenic differentiation of human bone marrow-derived mesenchymal stem cells. Chin Med Sci J. 2015;30:108–13.
42. Sadeghinia A, Davaran S, Salehi R, Jamalpoor Z. Nano-hydroxy apatite/chitosan/gelatin scaffolds enriched by a combination of platelet-rich plasma and fibrin glue enhance proliferation and differentiation of seeded human dental pulp stem cells. Biomed Pharmacother. 2019;109:1924–31.
43. Kawamura K, Yajima H, Ohgushi H, Tomita Y, Kobata Y, Shigematsu K, et al. Experimental study of vascularized tissue-engineered bone grafts. Plast Reconstr Surg. 2006;117:1471–9.